



Swansea University
Prifysgol Abertawe



Cronfa - Swansea University Open Access Repository

This is an author produced version of a paper published in:
Journal of Computational Design and Engineering

Cronfa URL for this paper:
<http://cronfa.swan.ac.uk/Record/cronfa31862>

Paper:

Zhang, L., Deng, A., Cameron, I., Wang, E. & Sienz, J. (2017). Parametric investigation on an industrial electromagnetic continuous casting mould performance. *Journal of Computational Design and Engineering*
<http://dx.doi.org/10.1016/j.jcde.2017.01.001>

This item is brought to you by Swansea University. Any person downloading material is agreeing to abide by the terms of the repository licence. Copies of full text items may be used or reproduced in any format or medium, without prior permission for personal research or study, educational or non-commercial purposes only. The copyright for any work remains with the original author unless otherwise specified. The full-text must not be sold in any format or medium without the formal permission of the copyright holder.

Permission for multiple reproductions should be obtained from the original author.

Authors are personally responsible for adhering to copyright and publisher restrictions when uploading content to the repository.

<http://www.swansea.ac.uk/library/researchsupport/ris-support/>



Contents lists available at ScienceDirect

Journal of Computational Design and Engineering

journal homepage: www.elsevier.com/locate/jcde

Parametric investigation on an industrial electromagnetic continuous casting mould performance

Lintao Zhang^{a,*}, Anyuan Deng^b, Ian Cameron^a, Engang Wang^{b,*}, Johann Sienz^a

^aAdvanced Sustainable Manufacturing Technologies (ASTUTE2020) Operation, College of Engineering, Swansea University, Bay Campus, Fabian Way, Swansea SA1 8EN, UK

^bKey Laboratory of Electromagnetic Processing of Materials (Ministry of Education) Northeastern University, No. 3-11, Wenhua Road, Shenyang 110004, PR China

ARTICLE INFO

Article history:

Received 2 November 2016
Received in revised form 28 December 2016
Accepted 9 January 2017
Available online 3 February 2017

Keywords:

Electromagnetic continuous casting
Finite element method
Taguchi method
Design of experiment
Analysis of variance

ABSTRACT

This research aimed at conducting a quantitative investigation of process parameters on the magnetic field contribution in an electromagnetic continuous casting mould. The Taguchi method (4 factors and 3 factor value levels: L9 orthogonal array) was adopted to design matrix of the simulation runs and the analysis of variance was used to evaluate the contributions of each control factor. The simulations were conducted based on the finite element method and the numerical set-up was validated by the designed experiment. The results showed that the applied alternating current magnitude contributed most (76.64%) to the magnetic field level in the mould, compared to the other control factors. It was followed by the slit length (17.72%), the alternating current frequency (4.17%) and the slit width (1.57%).

© 2017 Society for Computational Design and Engineering. Publishing Services by Elsevier. This is an open access article under the CC BY-NC-ND license (<http://creativecommons.org/licenses/by-nc-nd/4.0/>).

1. Introduction

The electromagnetic continuous casting (EMCC) technique was first applied in the aluminium casting (Vives & Ricou, 1985) and then the technique was adopted in steel making process (Yasuda, Toh, Iwai, & Morita, 1997). The depth of oscillation mark (OSM) on the billets was decreased from 0.45 (± 0.15) mm to 0.15 (± 0.05) mm (Park et al., 2003; Park, Jeong, Kim, & Kim, 2002) for 0.08–0.1% C steel (round billets) by using EMCC technique. For the square billets, similar results were obtained: OSM decreased from 0.65 mm to 0.06 mm (Xu, 2011). The improvement of billet surface quality simplified the following manufacturing process before the billets were rolled: the billets scalping process was avoided (Bermudez, Muniz, & Salgado, 2003). Therefore, the energy consumption was decreased.

The basic principle of EMCC technique was discussed by professor Vives (1985) and the metallurgy effect of this technique depends on several factors: the electric control and mould structure parameters, for instance. Therefore, the investigation on these issues are critical in terms of enhancing the mould performance. Plenty of research has been carried out to focus on the effect of

alternating current magnitude on the magnetic field level in the EMCC mould. The results unveiled that the magnetic field was enhanced as the current value was increased. A wide range of alternating current frequencies from 60 Hz (Toh, Takeuchi, Hojo, Kawai, & Matsumura, 1997) to 2500 Hz (Wang, 2009) and further to 100 kHz (Nakata, Inoue, Mori, Murakami, & Mominami, 2002) was investigated. The billet surface quality was improved for all the cases. However, for low frequency case, more fluctuations existed due to the electromagnetic stirring (EMS) effect. The EMCC mould (usually made of copper alloy) should have a slit-segment structure (“cold-crucible” structure) (Yasuda et al., 1997), which is due to the skin effect of copper under the high frequency electromagnetic field. The slit allows the magnetic field to permeate to the mould centre and act on the liquid steel. Zhou et al. experimentally studied the magnetic field distribution with different values of round mould slit width: 0.4 mm, 0.8 mm and 1.2 mm, respectively (Zhou, Zheng, Jun, Li, & Qu, 2001). Numerically, Zhang et al. investigated influence of the slit width (0.3 mm and 0.5 mm) on the magnetic field level in a round EMCC mould (Zhang, Wang, Deng, & He, 2006). Both studies showed that the magnetic field increased as the slit width value was increased, however, the uniformity of magnetic field along the circumferential direction may worsen. For the slit length, similar results were obtained for both square (Yu, Jia, Wang, He, Zhang, & Chen, 2002) and rectangular (Deng, Wang, He, Meng, Zhang, & Chen, 2003) EMCC mould: the magnetic field level was enhanced as the slit length values were increased.

Peer review under responsibility of Society for Computational Design and Engineering

* Corresponding authors.

E-mail addresses: L.Zhang@swansea.ac.uk (L. Zhang), egwang@mail.neu.edu.cn (E. Wang).

<https://doi.org/10.1016/j.jcde.2017.01.001>

2288–4300/© 2017 Society for Computational Design and Engineering. Publishing Services by Elsevier.

This is an open access article under the CC BY-NC-ND license (<http://creativecommons.org/licenses/by-nc-nd/4.0/>).

From the short literature review above, the research showed that the magnetic field level was in proportion to the applied alternating current magnitude, the slit width and length values, respectively. This raised a question:

- what is the exact quantitative contribution of the main control parameters on the magnetic field in the EMCC mould?

Little research has been conducted on this issue in the previous study. Answering the above question can help to figure out the contributions to the magnetic field of each parameters and therefore to find the most dominant one. The results could further help to design of experiments (DoE). That is the problem shall be tackled in the present research. The Taguchi method (Taguchi, 1985) basic principles discussed in Section 3.1 were used to design the simulation matrix. The reason for this selection was because that Taguchi method has been well validated in a wide field, e.g. for injection moulding process (Mehat & Kamaruddinb, 2011; Tang et al., 2007) and evaporative pattern casting process (Kumar, Kumar, & Shan, 2008).

The outline of the present paper is as follows. The configuration and numerical system are introduced Sections 2.1 and 2.2, respectively. To obtain the precise simulation results, an experimental validation for the numerical set-up is discussed in Section 2.3. In Section 3, a detailed Taguchi analysis is conducted. Main conclusions are summarised in Section 4.

2. Configuration and numerical system

2.1. Configuration

An industrial round EMCC mould supplied by a company, with an inner diameter 0.356 m, was adopted in the present research. The mould had a slit-segment structure and 32 slits were distributed equally along the circumference direction. Therefore,

Table 1
Material properties of the copper and steel.

Materials	Relative permeability (-)	Conductivity (S/m)	Density (kg/m ³)
Copper Fort, Garnich, and Ymyshyn (2005)	1	4.5×10 ⁷	8890
Steel Deng, Xu, Wang, and He (2014)	1	7.14×10 ⁵	7020

only 1/32 region (11.25°) of the EMCC mould system was investigated, as shown in Fig. 1. The dimensions (in millimetre) of the steel simulator, the mould and induction coil, along with their relative locations were also shown in the figure. The x- and y-axis are in the radial and the axial (casting) direction. I and II denote the symmetric surfaces of the steel simulator and the mould. III and IV denote the surfaces where applied alternating current flows in and out. The mould and induction coil were made of copper alloy and the steel simulator was made of stainless steel. The detailed material properties were listed in Table 1.

2.2. Numerical system

The simulations were conducted by Ansoft Maxwell® (version 16.0) based on finite element method. The simulation was based on the following assumptions (ANSYS Maxwell Online Help, 2012):

1. all the electromagnetic fields pulsate with the same frequency;
2. no moving objects in the simulation domain;
3. all the material properties are assumed to be linear.

The control equation for the conducting region can be expressed as follows (ANSYS Maxwell Online Help, 2012):

$$\nabla \times \left(\frac{1}{\sigma + j\omega\epsilon_0} \nabla \times \mathbf{H} \right) = j\omega\mu_0\mathbf{H}, \tag{1}$$

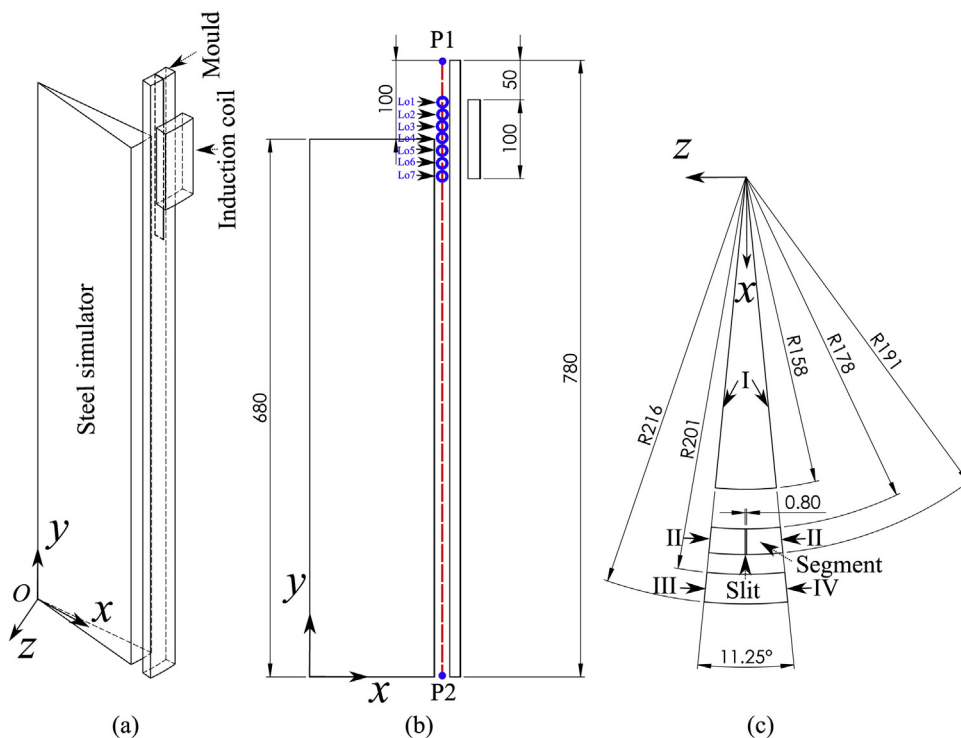


Fig. 1. The configuration of EMCC mould system: the steel simulator, the mould and the induction coil. 3D view (a), front view (b) and top view (c), respectively. I and II denote the symmetric surfaces of the steel simulator and the mould, respectively. III and IV denote the surfaces for the external applied alternating current in and out, respectively. Dimensions are in millimetre.

$$\omega = 2 \times \pi f, \quad (2)$$

where \mathbf{H} , σ , ω and f are the magnetic flux intensity (in Ampere per metre), the electric conductivity (in Siemens per metre), the angular frequency and the alternating current frequency, respectively. \mathbf{H} is calculated directly from the applied source current. For the non-conduction region, \mathbf{H} is computed from the magnetic scalar potential (ANSYS Maxwell Online Help, 2012):

$$\nabla \cdot (\mu \nabla \psi) = 0, \quad (3)$$

where ψ is magnetic scalar potential. The symmetry boundary condition (magnetic flux tangential) was applied on the surfaces I and II. For the induction coil, an alternating current \mathbf{I} was applied vertical to the symmetric planes (III and IV):

$$\mathbf{I} = I_m \cos(2\pi \cdot f \cdot t), \quad (4)$$

where I_m is the peak value of applied alternating current. Table 2 shows that the convergence was achieved after 8 iterations: the energy error value (0.0447%) at iteration 8 was smaller than the critical pre-set value 0.05%. The number of elements increased as the number of passes was increased. In the present simulation the

number of elements was 875,751. To obtain the precise results, the eddy current effect was also considered in electric conductive material, e.g. the mould. At least 4 elements were chosen within the skin depth. The meshes of steel simulator, the mould and induction coil are shown in Fig. 2.

2.3. Experiment validation

To further validate the numerical system in Section 2.2, an experiment aimed at measuring the magnetic field was designed and conducted. Fig. 3 shows the mould system adopted in the experiment. The round industrial mould (with slit-segment structure), the induction coil, the cooling water pipe and the tank were labelled, respectively. The mould was surrounded by a five-turn induction coil. The five-turn induction coil ensures the meniscus of the molten steel and the initial solidification region can be covered by the relatively strong magnetic field in the casting experiment, therefore to achieve the “soft-contact” effect (Deng et al., 2009; Xu et al., 2009). In the experiment, a solid stainless steel cylinder was used as a simulator of molten steel. In the experiment, the alternating current was supplied by an ISP-200 kW supersonic frequency power (frequency range: 10–50 kHz). The selected current frequency was 25 kHz in the experiment.

The small coil method (Gu & Lu, 1984; Ren, Dong, Deng, & Jiang, 2001; Zhang, Deng, Wang, & Sienz, 2016) was used to capture the magnetic field in the mould. A probe was first designed. The tip of probe was surrounded by a number of small copper coils. The small copper coils were connected with a voltage meter. The basic principle for the method can be understood as follows. The total magnetic flux, Φ , through the small coils is (Lorrain & Corson, 1979):

$$\Phi = N \cdot S \cdot \mathbf{B} \cos \theta, \quad (5)$$

where S , N , and θ are the cross sectional area, the number of the small coil turns, and the angle between the magnetic flux line and the normal direction of the coil, respectively. The magnetic flux density \mathbf{B} can be expressed as:

Table 2
The variation of energy error percentage and the total element number with the solution iterations.

Solution iterations	Energy error (%)	Element number
1	3.67	79,715
2	0.95	104,041
3	0.57	135,789
4	0.36	177,221
5	0.25	231,292
6	0.13	301,861
7	0.07	393,961
8	0.0447	514,160
9	0.024	671,026
10	0.014	875,751

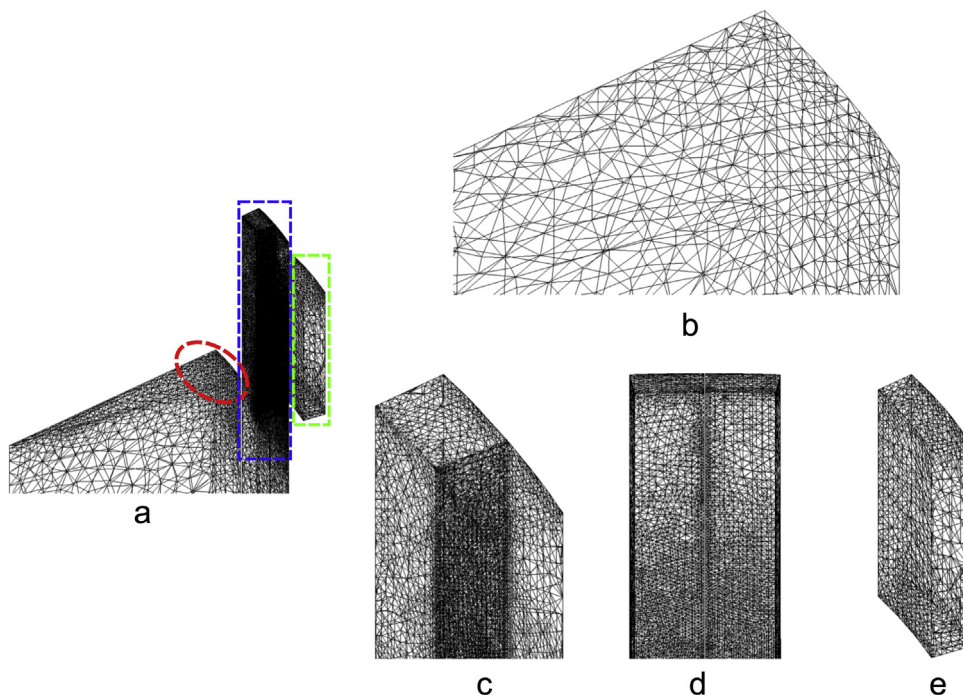


Fig. 2. The mesh of the steel simulator, the mould and the induction coil. (a) 3D view, (b) mesh of the steel simulator zone (within the red dashed line), (c) mesh of the mould zone (within the blue dashed line), (d) mesh of the mould zone y – z view and (e) mesh of the induction coil zone (within the green dashed line).

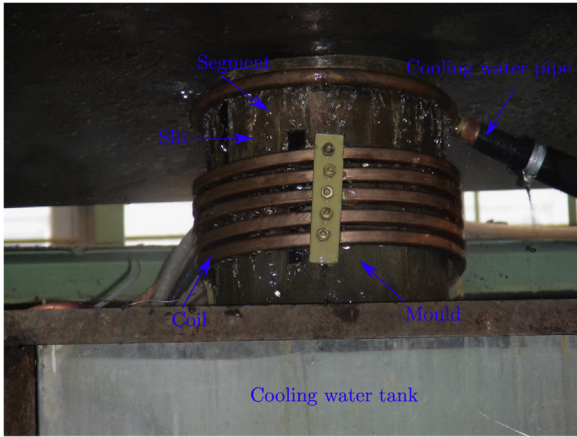


Fig. 3. The round EMCC mould system used in the experiment.

$$\mathbf{B} = B_m \sin(2\pi \cdot f \cdot t), \quad (6)$$

where B_m is the maximum magnitude of \mathbf{B} . Therefore, Eq. (5) can be rewritten as:

$$\Phi = N \cdot S \cdot B_m \sin(2\pi \cdot f \cdot t) \cos \theta. \quad (7)$$

Based on the Faraday induction law (Lorrain & Corson, 1979):

$$\oint \mathbf{E} \cdot d\mathbf{l} = -\frac{d\Phi}{dt} = -N \cdot S \cdot B_m \cdot \cos(2\pi f t) \cdot 2\pi \cdot f \cdot \cos \theta \\ = -E_m \cdot \cos(2\pi \cdot f \cdot t), \quad (8)$$

where

$$E_m = N \cdot S \cdot B_m \cdot 2\pi \cdot f \cdot \cos \theta. \quad (9)$$

For Eq. (9), E_m reaches the maximum value once $\theta = 0^\circ$. Therefore, E_{max} can be expressed as:

$$E_{max} = N \cdot S \cdot B_m \cdot 2\pi \cdot f. \quad (10)$$

The effective part of E_m can be expressed as follows:

$$E_{eff} = \frac{E_{max}}{\sqrt{2}}. \quad (11)$$

Therefore, Eq. (10) can be rewritten as:

$$B_m = \frac{\sqrt{2}E_{eff}}{2\pi \cdot f \cdot N \cdot S}. \quad (12)$$

In the equation, E_{eff} can be displayed by the voltage meter and f is the frequency of applied *a.c.* N and S are constants once the probe is designed. In the present experiment $N \times S = 1.712 \times 10^{-4} \text{ m}^2$. Therefore, the magnetic flux density can be calculated. The probe was placed between the outer surface of the steel simulator and the inner surface.

Fig. 4 shows the magnetic field distribution obtained from both simulation and experiment along the casting direction at the slit centre with a current density $2.13 \times 10^7 \text{ A/m}^2$.

The slit centre region was represented by a line between two points, $P1$ and $P2$, as shown in Fig. 1(b). The results showed that the magnetic field distribution follows the same trend along the casting direction. The maximum magnitude of B_y appeared almost at the same location (relative to mould top): -148 mm for experiment and -141 mm for simulation, respectively. Furthermore, the maximum B_y magnitudes were close: 0.081 T for experiment and 0.08 T for simulation, respectively. Therefore, the numerical set-up for the simulation was validated.

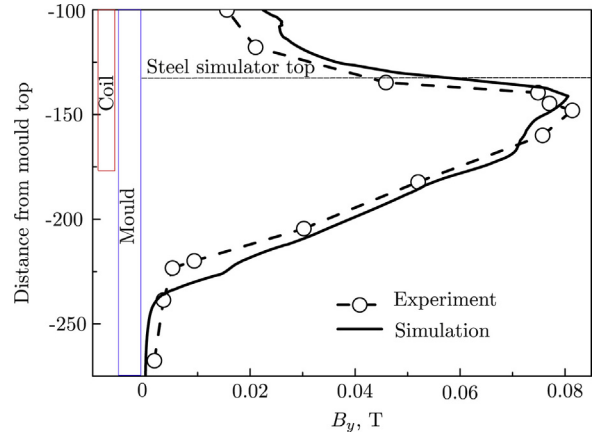


Fig. 4. Simulation and experiment results comparison of the magnetic flux density along casting direction in the vicinity of the slit region. The current density on the induction coil is $2.13 \times 10^7 \text{ A/m}^2$. The alternating current frequency is 25 kHz .

3. Taguchi method analysis

3.1. Basic principles of Taguchi method

The Taguchi method is a method used to optimise the engineering process and to improve the product quality (Taguchi, 1985, 1990). The method should be conducted in three steps in general: the system design, the parameter design and the tolerance design, respectively (Yang & Tarn, 1998). The product design, e.g. the material selection of the product, and the process design, e.g. the processing sequences, are the tasks that should be considered in the system design. The parameter design step of Taguchi method consists of the following steps (Nian, Yang, & Tarn, 1999; Xie & Yuan, 2016):

1. To identify the performance characteristics and select process parameters to be evaluated;
2. to determine the number of levels for the process parameters;
3. to select the appropriate orthogonal array (OA) and assignment of process parameters to the orthogonal array;
4. to conduct the experiments based on the arrangement of the orthogonal array;
5. to calculate the signal to noise (S/N) ratio;
6. to analyse the experimental results using the S/N ratio and ANOVA;
7. to select the optimal levels of process parameters;
8. to verify the optimal process parameters through the confirmation experiment.

For the present research, to answer the question raised in Section 1, the steps from 1 to 6 will be discussed in the following sections. The tolerance design is used to evaluate the tolerance around the optimised setting obtained by the parameter design.

3.2. Mould performance measurement and process parameter selection

The EMCC effect is achieved by the *soft-contact* behaviour between liquid metal and the mould (Vives, 1989). The soft-contact effect is depended on the level of Lorentz force, generated by the interaction between induced current in the molten metal and the magnetic field in the mould. Therefore, the mould performance was measured by the magnetic field level in the vicinity of steel simulator top (slit region) in the mould. In more detail, the

Table 3
The coordinates for Lo1 to Lo7.

Coordinates (mm)	Lo1	Lo2	Lo3	Lo4	Lo5	Lo6	Lo7
x	170	170	170	170	170	170	170
y	677.7	678.6	679.5	680.4	681.3	682.2	683.1
z	0	0	0	0	0	0	0

average value of y components (along casting direction) of the magnetic flux density, B_y , on the Lo1–Lo7 was selected as the performance characteristic. Lo1–Lo7 were shown in Fig. 1(b) and the detailed coordinates for Lo1–Lo7 were listed in Table 3.

Four process parameters were selected: the external applied A.C. value, the A.C. frequency, the slit width and length, respectively. They were named Factors A, B, C and D, respectively.

3.3. Process parameter level selection

For each control factor, three levels were selected. The details of control factors and their levels were summarised in Table 4.

3.4. Orthogonal array

The L9 (3^4) orthogonal array (OA) and the combination parameters for the control factors are shown in Table 5. Therefore, the detailed simulation conditions for the 9 trials were summarised in Table 6.

Table 4
The selected process parameter and their levels.

Control factor	Level 1	Level 2	Level 3
Current density, A/m ² (Factor A)	6.07×10^6	1.33×10^7	2×10^7
Frequency, kHz (Factor B)	20	30	40
Slit width, mm (Factor C)	0.3	0.5	0.8
Slit length, mm (Factor D)	150	180	210

Table 5
L9 orthogonal array.

Trial	Factor A	Factor B	Factor C	Factor D
1	1	1	1	1
2	1	2	2	2
3	1	3	3	3
4	2	1	2	3
5	2	2	3	1
6	2	3	1	2
7	3	1	3	2
8	3	2	1	3
9	3	3	2	1

Table 6
The combination parameters for the effective factors.

Trial	Current density, A/m ² (Factor A)	Frequency, kHz (Factor B)	Slit width, mm (Factor C)	Slit length, mm (Factor D)
1	6.07×10^6	20	0.3	150
2	6.07×10^6	30	0.5	180
3	6.07×10^6	40	0.8	210
4	1.33×10^7	20	0.5	210
5	1.33×10^7	30	0.8	150
6	1.33×10^7	40	0.3	180
7	2×10^7	20	0.8	180
8	2×10^7	30	0.3	210
9	2×10^7	40	0.5	150

3.5. Experiment conduction

According to Table 6, 9 trials of simulation were carried out and the results were obtained.

3.6. Signal–noise ratio calculation

The performance characteristic data (B_y) at Lo1–Lo7, for all the simulation trials, were listed in Table 7.

The larger-the-better of signal–noise ratio was adopted because that the EMCC mould system was expected to respond as large as possible. For the larger the better (LB), S/N can be expressed (Phadke, 1989; Taguchi, 1985; Taguchi, Chowgdhury, & Wu, 2004):

$$(S/N)_L = -10 \cdot \log \left(\frac{1}{n} \sum_{i=1}^n \frac{1}{y_i^2} \right). \tag{13}$$

In the equation, y is the performance characteristic data (B_y) and n is the number of the data collecting point (7 in the present research) in a single simulation trial. The averaged B_y , $\overline{B_y}$, and the S/N ratios were calculated and summarised in Table 8.

3.7. Signal–noise ratio analysis

Therefore, based on the S/N ratios, the average S/N ratio in terms of the different control factors, A–D, at different levels, 1–3, was summarised in Table 9. The ranks are difference between the maximum value of S/N ratio and the minimum ratio at different levels for each factor.

The S/N response diagram is shown in Fig. 5. It showed that the best combination for the experiment parameters should be A_3, B_1, C_3 and D_3 , respectively. A further analysis was carried out by using analysis of variance (ANOVA) method. The details of degree of freedom (DoF), sum of square (SS) factor, variance and percentage contribution were calculated by the following methods (Tang et al., 2007), respectively. For the total degree of freedom:

$$f_T = N - 1, \tag{14}$$

where N is the total number of the simulation trial. For each control factor:

$$f_j = k_j - 1, \tag{15}$$

where j denotes Factors A, B, C and D, respectively. f_j and k_j denote the freedom and the levels of factors A, B, C and D, respectively. The total sum of square S_T can be calculated by the following equation:

$$S_T = \sum_{i=1}^9 (y_{ia}^2) - \frac{1}{9} \sum_{i=1}^9 (y_{ia})^2, \tag{16}$$

where y_{ia} is the $\overline{B_y}$ for the selected locations (Lo1–Lo7) for the simulation trial i , where $i \in [1-9]$. For each control factor:

Table 7

B_y values at Lo1 to Lo7 for simulation trial 1 to 9.

Trial	B_y , mT						
	Lo1	Lo2	Lo3	Lo4	Lo5	Lo6	Lo7
1	17.40	17.28	17.12	16.96	16.78	16.64	16.51
2	27.94	27.67	27.39	27.04	26.63	26.20	25.75
3	35.20	34.82	34.42	33.95	33.43	32.88	32.25
4	66.98	66.12	65.23	64.33	63.42	62.49	61.47
5	42.30	42.03	41.72	41.40	41.06	40.67	40.25
6	47.24	46.73	46.18	45.53	44.90	44.27	43.62
7	91.68	90.68	89.63	88.51	87.25	86.00	84.74
8	89.54	88.42	87.23	86.00	84.68	83.31	81.89
9	54.86	54.47	54.15	53.82	53.19	52.50	51.84

Table 8

Performance characteristic data \bar{B}_y and S/N ratios.

Trial	A	B	C	D	\bar{B}_y , mT	S/N
1	1	1	1	1	16.96	24.58
2	1	2	2	2	26.95	28.60
3	1	3	3	3	33.85	30.58
4	2	1	2	3	64.29	36.15
5	2	2	3	1	41.35	32.33
6	2	3	1	2	45.49	33.15
7	3	1	3	2	88.35	38.92
8	3	2	1	3	85.87	38.67
9	3	3	2	1	53.55	34.57

Table 9

The response table of S/N for the current values, the current frequency, the slit width and slit length, respectively. The bold values denote the maximum S/N values.

Factors	Level 1	Level 2	Level 3	Rank
Current, A (Factor A)	27.92	33.78	37.38	9.46
Frequency, kHz (Factor B)	33.22	33.20	32.77	0.43
Slit width, mm (Factor C)	32.13	33.02	33.94	1.81
Slit length, mm (Factor D)	30.49	33.56	35.04	4.55

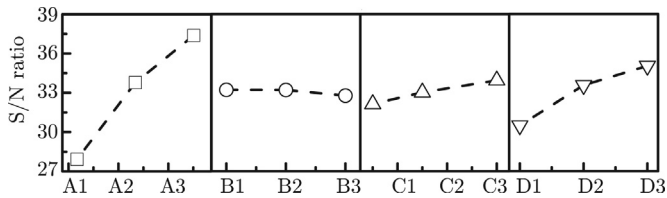


Fig. 5. The response diagram of S/N ratios for current value (Factor A), current frequency (Factor B), slit width (Factor C) and slit length (Factor D), from left to right, respectively.

$$S_j = \frac{1}{k_j} \sum_{m=1}^{k_j} (y_{ma}^2) - \frac{1}{9} \sum_{i=1}^9 (y_{ia})^2, \quad (17)$$

where y_{ma} is \bar{B}_y at m level for control factor j , where $m \in [1-3]$. The variance and the percentage contribution of the control factors can be obtained by the following equations:

$$V_j = \frac{S_j}{f_j} \quad (18)$$

and

$$P_j = \frac{S_j}{S_T} \times 100. \quad (19)$$

The detailed data for DoF, SS, variance and P were summarised in Table 10. Fig. 6 further shows the contribution percentage of each control factors on the magnetic field level in the mould. The percentage contributions of the current, the electric frequency, the slit width and the slit length are 76.64%, 4.17%, 1.57% and 17.62%, respectively. Unsurprisingly, the current has most dominant effect on the magnetic field in the mould and slit width has least influence, compared to the other three control factors.

Table 10

The Analysis of Variance (ANOVA) table. DoF, SS, and P denote degrees of freedom, sum of squares, and the percentage sum of squares, respectively.

Source of variation	DoF	SS	Variance	$P(\%)$
Current, A	2	3753.81	1876.91	76.64
Frequency, kHz	2	204.22	102.11	4.17
Slit width, mm	2	77.10	38.55	1.57
Slit length, mm	2	863.05	431.53	17.62
Total	8	4898.19	-	100

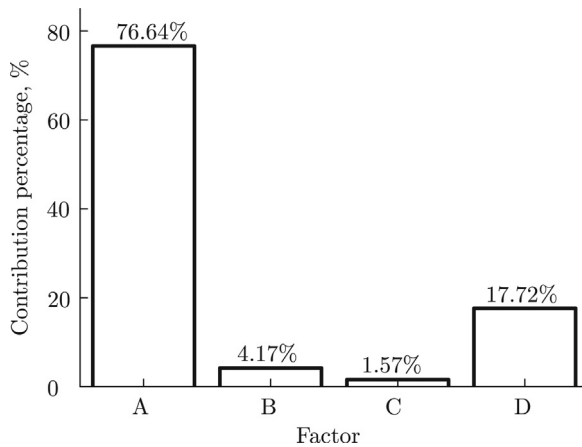


Fig. 6. Contribution percentage on each control factors.

4. Conclusions

A quantitative analysis, aimed at investigating the contributions of applied alternating current, the current frequency, the mould slit width and slit length to the magnetic field level in EMCC mould, was conducted. Therefore, the question raised in Section 1 was answered and the main conclusions were summarised as follows:

- The numerical system was validated by the designed experiment. This indicated that the simulation results were reliable and be used to guide the further experimental design.
- For all the selected control factors, the alternating current value was the most influential factor. It showed a contribution rate, to the magnetic field level, of 76.64%. The second most influential factor was the slit length at 17.72%, followed by the current frequency at 4.17%. The least influential factor was slit width at 1.57%.
- The Taguchi orthogonal array reduced the number of trials in experiment design. Based on the results obtained, more consideration should be given to slit length compared to the slit width and current frequency during the following EMCC mould design.

Acknowledgements

The authors would like to acknowledge Advanced Sustainable Manufacturing Technologies (ASTUTE2020) Operation part-funded by the European Regional Development Fund (ERDF) through the Welsh Government. The authors are also gratefully acknowledge the financial support from the National Nature Science Foundation of China (Grants 51574083 and 51474065). The authors are grateful to Professor Alban Potherat for fruitful discussion with him during the conduct of this work. Furthermore, the authors would also like to thank the reviewers for their work which has contributed to this paper.

References

ANSYS Maxwell Online Help (2012). *Maxwell 3D technical notes: Frequency domain (eddy current) solver*, v16.0. SAS IP, Inc.

Bermudez, A., Muniz, C. M., & Salgado, P. (2003). Asymptotic approximation and numerical simulation of electromagnetic casting. *Metallurgical and Materials Transactions B*, 34B, 83–91.

Deng, A., Wang, E., He, J., Meng, G., Zhang, Y., & Chen, Z. Z. (2003). Experimental study of distribution of magnetic flux in rectangular soft-contact mold. *Acta Metallurgica Sinica*, 39(10), 1105–1109.

Deng, A., Xu, L., Wang, E., & He, J. (2014). Numerical analysis of fluctuation behaviour of steel/slag interface in continuous casting mold with static magnetic field. *International Journal of Iron and Steel Research*, 21(9), 809–816.

Deng, A. Y., Xu, X. J., Wang, E. G., Zhang, L. T., Zhang, X. W., & He, J. C. (2009). Experimental research on round steel billet electromagnetic soft contact continuous casting process. *Iron & Steel*, 44(4), 33–37.

Fort, J., Garnich, M., & Ymyshyn, K. (2005). Electromagnetic and thermal-flow modeling of a cold-wall crucible induction melter. *Metallurgical and Materials Transactions B*, 36B, 141–152.

Gu, C., & Lu, Q. (1984). On the point-value measurement of the inhomogeneous magnetic field. *Acta Metrologica Sinica*, 5(2), 131–136.

Kumar, S., Kumar, P., & Shan, S. H. (2008). Optimization of tensile properties of evaporative pattern casting process through Taguchis method. *Journal of Materials Processing Technology*, 204, 59–69.

Lorrain, Paul, & Corson, Dale R. (1979). *Electromagnetism: Principles and applications* (1st printing ed.). W.H. Freeman & Co Ltd. April.

Mehat, M. N., & Kamaruddin, S. (2011). Optimization of mechanical properties of recycled plastic products via optimal processing parameters using the Taguchi method. *Journal of Materials Processing Technology*, 211, 1989–1994.

Nakata, H., Inoue, T., Mori, H., Murakami, T., & Mominami, T. (2002). Improvement of billet surface quality by intra-high-frequency electromagnetic casting. *ISIJ International*, 42(3), 264–272.

Nian, Y. C., Yang, H. W., & Tarn, S. Y. (1999). Optimization of turning operations with multiple performance characteristics. *Journal of Materials Processing Technology*, 95, 90–96.

Park, J., Jeong, H., Kim, H., & Kim, J. (2002). Laboratory scale continuous casting of steel billet with high frequency magnetic field. *ISIJ International*, 42(4), 385–391.

Park, J., Kim, H., Jeong, H., Kim, G., Cho, M., Chung, J., ... Cho, J. (2003). Continuous casting of steel billet with high frequency electromagnetic field. *ISIJ International*, 43, 813–819.

Phadke, S. M. (1989). *Quality engineering using robust design*. Englewood Cliffs, NJ 07632: PTR Prentice Hall.

Ren, Z., Dong, H., Deng, K., & Jiang, G. (2001). Influence of high frequency electromagnetic field on the initial solidification during electromagnetic continuous casting. *ISIJ International*, 41(9), 981–985.

Taguchi, G. (1985). Quality engineering in Japan. *Bulletin of the Japan Society of Precision Engineering*, 19(4), 237–242.

Taguchi, G. (1990). *Introduction to quality engineering*. Tokyo: Asian Productivity Organization.

Taguchi, G., Chowdhury, S., & Wu, Y. (2004). *Taguchi's quality engineering handbook* (1st ed.). John Wiley & Sons. 19 Nov.

Tang, S. H., Tan, J. Y., Sapuan, M. S., Sulaiman, S., Ismail, N., & Samin, R. (2007). The use of Taguchi method in the design of plastic injection mould for reducing warpage. *Journal of Materials Processing Technology*, 182, 418–426.

Toh, T., Takeuchi, E., Hojo, M., Kawai, H., & Matsumura, S. (1997). Electromagnetic control of initial solidification in continuous casting of steel by low frequency alternating magnetic field. *ISIJ International*, 37(11), 1112–1119.

Vives, C. (1989). Electromagnetic refining of aluminum alloys by the CREM process: Part I. Working principle and metallurgical results. *Metallurgical and Materials Transactions B*, 20, 623–629.

Vives, C., & Ricou, R. (1985). Experimental study of continuous electromagnetic casting of aluminum alloys. *Metallurgical and Materials Transactions B*, 16B, 377–384.

Wang, Z. (2009). *Studies of soft-contact electromagnetic continuous casting process under intermediate frequency electromagnetic field*. Shenyang, China: Northeastern University.

Xie, J., & Yuan, C. (2016). Parametric study of ice thermal storage system with thin layer ring by Taguchi method. *Applied Thermal Engineering*, 98, 246–255.

Xu, X. (2011). *Research on the mechanism of quality improvement of continuous casting billet by high frequency electromagnetic field and industrialization*. Shenyang, China: Northeastern University.

Xu, X. J., Deng, A. Y., Wang, E. G., Zhang, L. T., Zhang, X. W., Zhang, Y. J., ... He, J. (2009). Evolution mechanism of surface oscillation marks on the round billet during soft-contact electromagnetic casting. *Acta Metallurgica Sinica*, 45(4), 464–469.

Yang, H. W., & Tarn, S. Y. (1998). Design optimization of cutting parameters for turning operations based on the Taguchi method. *Journal of Materials Processing Technology*, 84, 122–129.

Yasuda, H., Toh, T., Iwai, K., & Morita, K. (1997). Recent progress of EPM in steelmaking, casting, and solidification processing. *ISIJ International*, 47(4), 619–626.

Yu, G., Jia, G., Wang, E., He, J., Zhang, Y., & Chen, Z. (2002). High frequency magnetic field distribution in region of initial solidification within soft contact electromagnetic continuous casting mold of billet. *Acta Metallurgica Sinica*, 38 (2), 208–214.

Zhang, L., Deng, A., Wang, E., & Sieng, J. (2016). An experimental investigation to facilitate an improvement in the design of an electromagnetic continuous casting mould. *Processes*, 14(4), 1–13.

Zhang, L., Wang, E., Deng, A., & He, J. (2006). Numerical simulation of influence of slit parameters of soft-contact mould on the distribution of magnetic field. *The Chinese Journal of Process Engineering*, 6(5), 713–717.

Zhou, Y., Zheng, X., Jun, J., Li, T., & Qu, F. (2001). Experimental study of influence of structure of soft-contacting mold on distribution of magnetic field. *Journal of Dalian University of Technology*, 41(6), 691–695.